J. Phys. B: At. Mol. Opt. Phys. **33** (2000) 3615–3630. Printed in the UK PII: S0953-4075(00)50344-7

Electron impact dissociative ionization of the CH_2F_2 molecule: cross sections, appearance potentials, nascent kinetic energy distributions and dissociation pathways

I Torres†, R Martínez‡, M N Sánchez Rayo† and F Castaño†§

† Departamento de Química Física, Universidad del País Vasco, Facultad de Ciencias, Apart. 644, 48080 Bilbao, Spain

‡ Facultad de Farmacia, Paseo de la Universidad, 7, 01006 Vitoria, Spain

E-mail: qfpcaalf@lg.ehu.es (FC)

Received 20 March 2000, in final form 13 July 2000

Abstract. Ions produced by crossed-beam collisions of pulsed monoenergetic electrons and supersonic expansion molecules have been analysed by time-of-flight mass spectroscopy (TOF-MS) in order to determine the appearance potentials, absolute total, dissociative and parent ionization cross sections and nascent ion kinetic energy distributions. The electron impact study was conducted at incident electron energies up to 100 eV on the parent CH_2F_2 molecule (and Ar/CH_2F_2 mixtures), a fluoromethane where the CH_2F^+ ion is produced at higher yields (1:18) than the parent molecule ion, $CH_2F_2^+$. TOF-MS band profiles analysis has enabled us to determine the ions' nascent kinetic energy distributions, information that combined with the dissociative ionization appearance potentials, calculated molecular orbital energies and orbital bond characters, leads to improved identification of the electron impact dissociative channels.

1. Introduction

The family of fluoromethane molecules has a number of combined properties which are useful in practical and industrial applications, particularly in high-energy systems with fast molecular energy transfer or efficient surface chemical attack. The release of ground-state and electronically excited atomic fluorine, fluorine ions and carbene radicals upon electron/ion impacts in addition to their very low boiling points (a consequence of the weak intermolecular interactions in the ground state) make them particularly interesting. The production of highly reactive fragments and ions yields efficient plasmas to initiate chemical attack on low reactive surfaces and quickly propagating gas reactions (Roth 1995). Semiconductor etching and the terrestrial ionosphere are well known systems where fluoromethanes play an important role (Moss and Ledwith 1987, Wayne 1991).

Crucial to the modelling of fluoromethane plasmas and to potential industrial uses is the knowledge of the excitation, total, dissociative and parent ionization cross sections, appearance potentials (AP or appearance energies, AE) and dissociation branching ratios. In dissociative processes the ionization channels are commonly identified by matching the thermodynamic computed enthalpies and the appearance potentials. The comparison always results in the same pattern: computed enthalpies are consistently lower for a few eV than the experimental

§ Author to whom correspondence should be addressed.

0953-4075/00/183615+16$30.00

AP. Although the energy difference is accepted as being located as fragment kinetic energies, the broad energy range and the lack of well defined correlations with other physical properties makes it difficult to sensibly justify channel assignments. This paper applies the nascent kinetic energy distributions (KEDs) obtained in a commercially available time-of-flight mass spectroscopy (TOF-MS) system, to ascertain the ionization pathways and to correlate them to the ion masses and bond dissociation energies.

Due to their practical applications, fluoromethanes have been the subject of a considerable number of papers, recently reviewed for the widely used CF_4, CHF_3 and CCl_2F_2 molecules (Christophorou *et al* 1996, 1997a, b) and other industrially interesting fluorine derivatives such as C_2F_6, C_3F_8 (Christophorou *et al* 1998a, b), NF_3 and SF_6 (Tarnovsky *et al* 1994, 1998). The reported data on total and dissociative ionization cross sections often have discrepancies of greater than 20% and the studies have not been extended to other potentially useful fluoromethanes, such as CH_2F_2. Cross section discrepancies are even more significant for lighter ions where the large kinetic energy produces a loss of collected ions and influences the appearance energy.

In previous works, optical emission from electronic excited neutrals and ions produced by electron impact on bulk CH_2F_2 was analysed, and emission cross sections, emission thresholds and lifetimes of electronically excited CF, CF_2, CH, CH^+ and F I were reported (Martínez *et al* 1993, Torres *et al* 1999). This work reports a further investigation on CH_2F_2 electron impact ionization, prepared in a pulsed supersonic beam and analysed by TOF-MS spectroscopy. The system was calibrated with N_2, Ar and CF_4 as reference gases and the TOF-MS band profiles modelled in order to obtain the ions' kinetic energy distributions, which further combined with APs, yields a quantitative identification of the ion channel pathways. The electron energy range studied was from appearance potentials up to 100 eV, a region where most molecule fragmentation channels are opened and the ionization cross section usually reaches its maximum value.

2. Experimental

2.1. General description

The experimental set-up used is built around a linear two-field Wiley–McLaren (Wiley and McLaren 1955) TOF-MS (R M Jordan Co.), equipped with both a pulsed molecular supersonic and a monoenergetic electron beam crossed at right angles in an originally electric field-free volume (figure 1). The vacuum chamber system itself consists of three well defined regions referred to as ionization/extraction, acceleration and flight tube/MCP detector. 300 ns after electron–molecule collisions take place in the extraction region, a 180 V negative pulse is applied to the extraction grid, creating an electric field that drives the ions onto the acceleration region, where a biased field of 1400 V cm^{-1} drives the ions further into the 86.5 cm long flight tube, where a couple of x–y plates focus the ions onto a three-stage microchannel plate (MCP) detector (C-0701, $\varnothing = 18$ mm). The ionization region repeller plate and extraction grid are 1.27 cm apart so that the effective electric field applied was $\sim$146 V cm^{-1}. The detector response is routed to a digital oscilloscope (Tektronix TDS360) and subsequently to a computer for further analysis and storage.

Electrons are generated in a standard heated W-pin filament and subsequently accelerated at a predetermined energy, collimated and focused by two electron lenses controlling the beam spread in the ionization region. A well focused beam is estimated to be ~ 3 mm in diameter. There is an additional third lens divided into two equal semicircular pieces, in contact with the repeller plate and the extraction grid, respectively, so that the same voltage applied to the

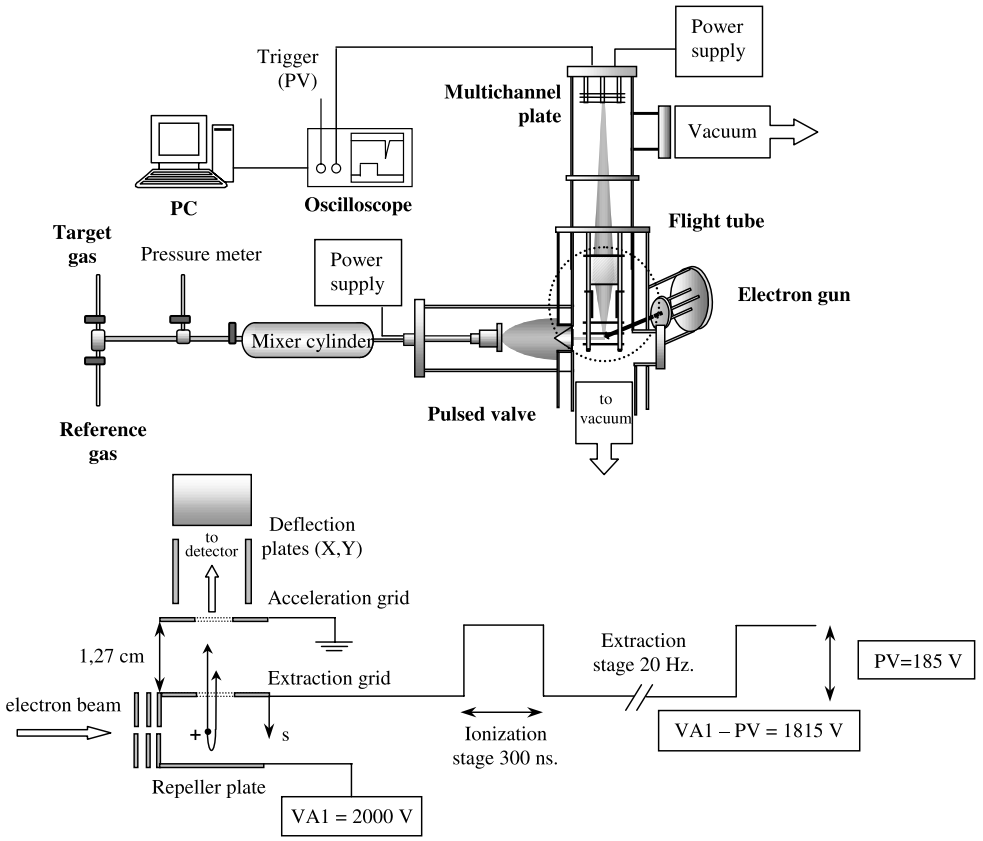

Figure 1. Schematic representation of the experimental set-up used to determine the ionization cross section, the appearance potential and the ion kinetic energy distributions. The TOF ion extraction and acceleration regions of the system are also indicated. The pulsed valve, the electron gun and the voltage extraction pulse have been appropriately delayed to optimize the multichannel plate detector signals.

plates biases the whole excitation region. The electron energy is varied in the 0–100 eV range and was calibrated with the Ar^+ appearance potential (15.75 eV) to an accuracy of better than ± 0.7 eV. The electron gun spread depends on the filament heating current and is estimated to be 1 eV at 100 μA electron intensity. In order to narrow the electron energy spread the AP measurements were carried out at only 1 μA electron intensity, where the accuracy is estimated to be ± 0.5 eV.

Reference and target gases were mixed in a high-pressure external stainless steel cylinder and the total pressure measured with a capacitance manometer (MKS-Baratron 750B) to 1% accuracy. The cylinder was directly connected to an 0.8 mm $\varnothing$ nozzle pulsed valve (General Valve, mod. IOTA ONE) from which the expansion proceeds to the main vacuum chamber ($<10^{-7}$ mbar), producing the supersonic beam; the valve open control pulse is used, with 600 μs delay, as the extraction grid trigger that further drives the ions towards the acceleration stage. The beam central and uniform region is skimmed ($\varnothing = 1$ mm) at a distance of 5 cm from the nozzle head, where the parent molecule degrees of freedom are frozen, and consequently the AP measurements are more reliable, the channel analysis is simplified and data acquisition is easier and faster (Syage 1988).

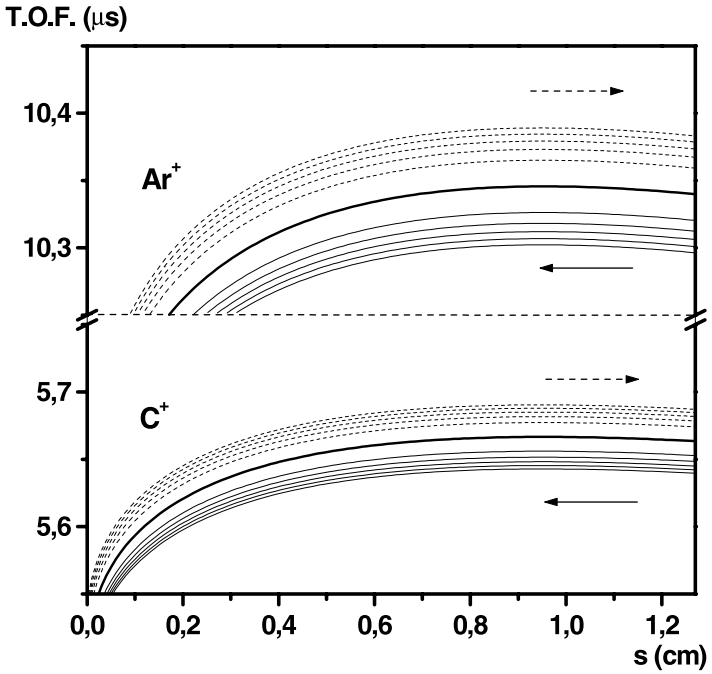

Figure 2. Simulated TOF of Ar^+ (40 amu) and C^+ (12 amu) ions as a function of the ionization space position with respect to the extraction plate, s. Curves above and below the nascent zero kinetic energy, $U_0 = 0$ eV (bold curve), refer to ions with velocity directed outwards from (broken curves) and towards (full curves) the extraction plate, respectively. The energy increase between any two adjacent curves is 0.1 eV.

2.2. Ion kinetic energy distributions and absolute total cross sections

The TOF-MS band profile depends mainly on both the nascent ion positions with respect to the extraction plate (Wiley and McLaren 1955) and their kinetic energies (Franklin *et al* 1967, Schäfer *et al* 1991). Indeed, and as an example, figure 2 shows the modelled Ar^+ (40 amu) and C^+ (12 amu) ion trajectories TOFs in our system as a function of the ion initial distance to the extraction plate (s, in cm); the bold curves correspond to zero kinetic energy ions and the others to ions with velocities directed to (full curves) and from (broken curves) the MCP detector, at 0.1 eV kinetic energy steps. A comparison of the theoretical and the experimental bandwidth with variable extraction pulses permits us to locate the beam-crossing distance to the extraction grid at about 0.9 ± 0.05 cm, a position where the bandwidth is insensitive to the space position and thus the ion kinetic energy is the main factor influencing the band profile. The method has a significant advantage with respect to those extraction designs where energy resolution is improved by setting a delay between the ion formation and the extraction pulse at the expense of space resolution (Wiley and McLaren 1955). However, it is unavoidable that during the initial 300 ns the ions travel according to their nascent velocities following the arrows shown in figure 2. Ions travelling away from the detector will not significantly change their TOF, while those moving towards the detector will approach the extraction plate following the full lines (figure 2) and will reduce the space resolution as they are delayed. The effect is mirrored in TOF-MS asymmetric bands, with a tail on the band short time and leaving unperturbed the long time side, thus providing reliable KEDs. Decreasing the ionization delay at the expense of a lower ion yield may reduce band asymmetry.

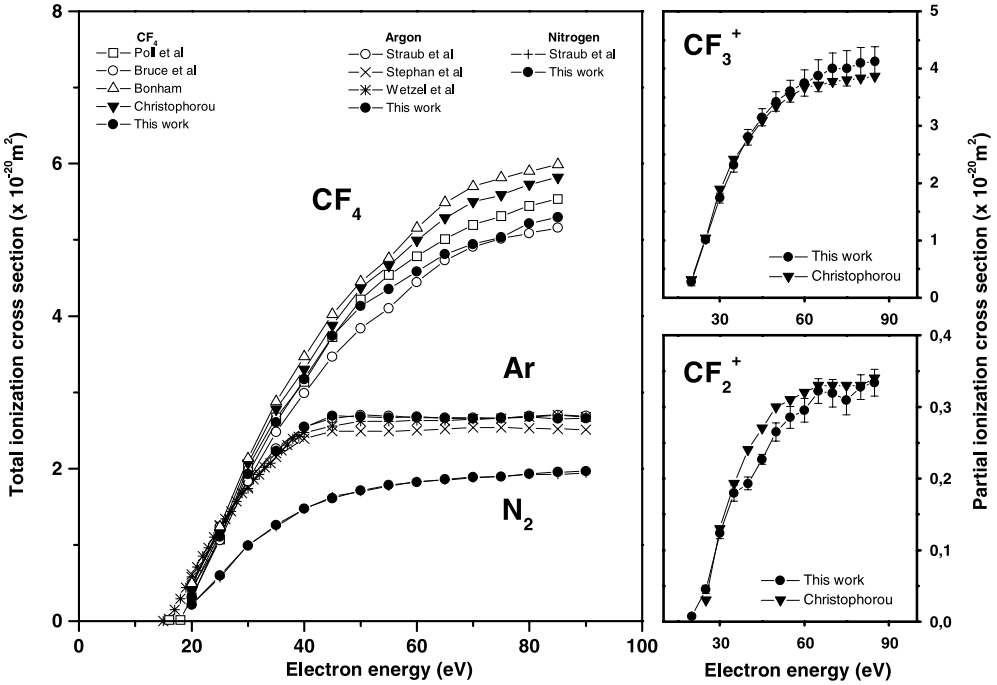

Figure 3. Absolute ionization cross sections system calibration. Comparisons are as follows. For the Ar^+ ion: ○, data reported by Straub *et al* (1995); ×, Stephan *et al* (1980); ∗, Wetzel *et al* (1987); ●, this work. For the N_2^+ ion: +, values from Straub *et al* (1996); ●, this work. For CF_4 data: □, from Poll *et al* (1992); ○, Bruce *et al* (1993), △, Bonham (1994); ▼, Christophorou *et al* (1996); ●, this work.

The optimization of the space-focusing condition is obtained by adjusting the electric field ratio in the acceleration and extraction regions, observed experimentally by plotting the TOF-MS FWHM peaks as a function of the extraction pulse voltage (PV). The focusing conditions are independent of the ion and its kinetic energy, 185 V being the optimum value for an acceleration biased voltage of 2000 V. Optimized voltages result in narrower and more intense TOF MS peaks. These experimental voltages agree very well with the series expansion of an ion TOF formed with zero kinetic energy at a distance s from the extraction plate in the neighbourhood of the excitation region centre, s_0 ($T(0, s)$ in Wiley and McLaren's (1955) notation) and also with the calculations carried out with the 'SIMION 3D' software (1987).

Nascent kinetic energy distributions, $n(U(t))$, are readily worked out from the TOF band profiles, $f(t)$, according to the relationship (Schäfer *et al* 1991):

$$n(U(t)) = \frac{2m}{(qE)^2}\frac{\mathrm{d}f(t)}{\mathrm{d}t} \tag{1}$$

where E is the electric field in the ionization region (146 V cm^{-1} in the experiments) and m is the ion mass with charge q.

CH_2F_2 absolute ionization cross sections were calibrated with Ar (40 amu) and CF_4 as a close mass reference gas, thus minimizing the mass effect. The ionization cross section for any B^+ fragment ion, is obtained from

$$\sigma_{B^+}(E) = \frac{I_{B^+}n_{Ar}}{I_{Ar^+}n_{CH_2F_2}}\sigma_{Ar^+}(E) \tag{2}$$

where I_B^+ and I_{Ar}^+ are the B^+ and Ar^+ detector currents, σ_{Ar}^+ is the reference ionization cross section, n_{Ar} and $n_{CH_2F_2}$ are the Ar and CH_2F_2 gas densities, which are assumed to be proportional to the external cylinder initially prepared mixture pressures (Syage 1988). In order to check the accuracy of equation (2) in our experiments, N_2 and Ar single-ionization cross sections were compared with each other using the reliable values reported by Straub *et al* (1995) (figure 3). For completeness purposes, the Ar^+ ionization cross sections reported by Stephan *et al* (1980) and Wetzel *et al* (1987) have been included in the plot and the agreement is excellent. The ionization cross section determination process has been analysed by Syage (1988) and, despite the internal standard value dependence, it has advantages. In fact, provided that sample and reference m/q ratios are alike, effects such as ion extraction from the ionization region, focusing on the MCP and detector gain factors are minimized. CF_4 cross sections were also measured to estimate the accuracy of the CH_2F_2 ones and the results are compared in figure 3 with those reported elsewhere (Poll *et al* 1992, Bonham 1994, Bruce and Bonhan 1993, Christophorou *et al* 1996). The spread of the CF_4 reported cross sections makes it safer to use the reliable Ar^+ and N_2^+ ions cross sections. CF_3^+ and CF_2^+ dissociative ionization cross sections are also shown in figure 3 and compared with Christophorou's recommended values.

3. Results and discussion

3.1. Cross sections

The parent CH_2F_2 TOF mass spectrum effected by 70 eV electron impact on a pulsed supersonic expansion is shown in figure 4, and is similar to that obtained in the CH_2F_2/Ar 1:1 mixture

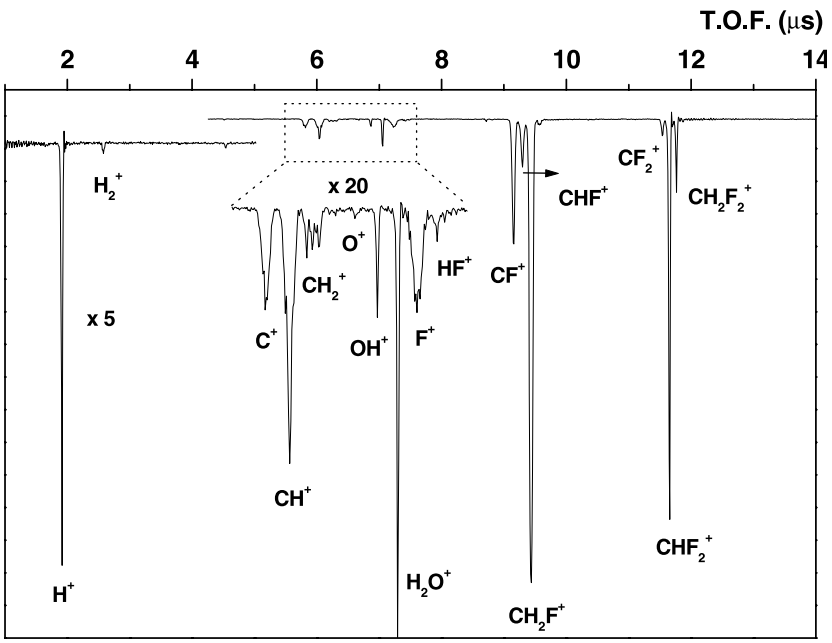

Figure 4. Mass-resolved TOF spectrum effected by 70 eV electron impact on the CH_2F_2 parent molecule. Note that some ion peaks split into several bands (CH_2^+, F^+). Peaks appearing at 6.86 and 7.05 μs correspond to OH^+ and H_2O^+ ions, respectively, and indicate the presence of water vapour in the system.

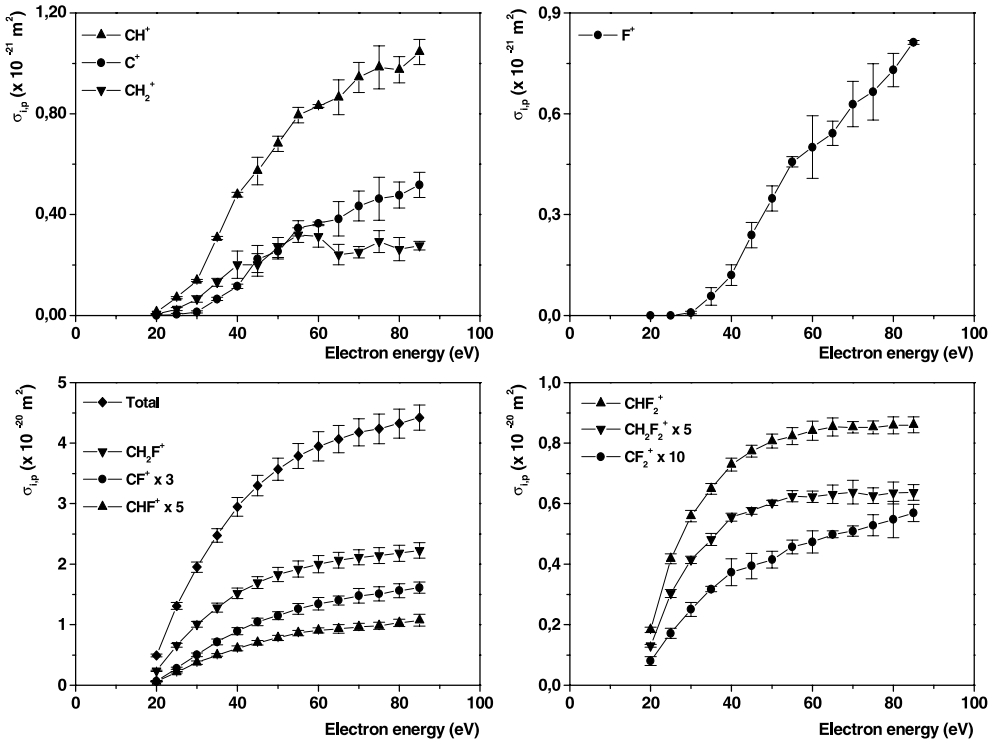

Figure 5. Absolute partial and total electron-impact ionization cross sections of CH_2F_2 as a function of the electron incident energy. Overall errors are estimated to be better than ±10% for ions with masses close to that of the reference (Ar), and increase to 15–20% for lighter fragments due to their high kinetic energies.

expansion. Neither $[CH_xF_{4-x}]_n^+$: $[Ar]_m^+$ nor Ar_n^+ clusters are observed in the TOF mass spectrum and thus their contributions to the ionization cross sections are considered negligible. Contributions from ion clusters appearing at TOF above 14 μs have been proved to disappear at stagnation pressures below 1.5 atm. Observed peaks at 7.05 and 6.86 μs are attributed to H_2O^+ and OH^+ ions, revealing the presence of water traces in the expansion mixture, a fact affecting the H^+ and H_2^+ ionization cross section measurements, whose data were corrected using reported values of the H_2O ionization cross sections (Straub *et al* 1998).

It is well established that the dissociation or predissociation channels in preference to electronic excitation dominate fluoromethane electron impact ionization. In the case of CF_4 and CHF_3, the CF_4^+ and CHF_3^+ ions have not been detected and emission from their excited states is doubtful (Christophorou *et al* 1996, 1997a), whereas CH_2F_2 yields a stable ion. Nonetheless, the most abundant ion following CH_2F_2 electron bombardment is CH_2F^+, with a cross section at high energies 18 times higher than that for $CH_2F_2^+$. In figure 5 and table 1 the CH_2F_2 total counting and dissociative ionization cross sections of 20–85 eV electron impact energies are collected, a range where the double-ionization processes contribute only negligibly to the observed total ionization cross section.

Errors in the dissociative ionization cross section measurements are basically due to the uncertainty of the reference cross section (3.5%, Straub *et al* 1995) and to the electron impact energy, estimated to be, once the system has been calibrated with the Ar^+ AP, less than ±1 eV. Larger errors are expected for lighter fragments, such as H^+ and H_2^+, since the detector is

Table 1. Partial and total ionization cross sections of ions produced by electron impact on CH_2F_2 (cross sections are in units of 10^{-21} m^2).

E_e (eV)	C^+	CH^+	CH_2^+	F^+	HF^+	H^+	H_2^+
20	0	0.01	0.01	0	—	0.025	—
25	0	0.07	0.03	0	0.004	0.073	0.003
30	0.01	0.14	0.07	0.01	0.005	0.128	0.006
35	0.07	0.31	0.13	0.06	0.013	0.215	0.008
40	0.12	0.48	0.2	0.12	0.017	0.380	0.012
45	0.22	0.57	0.2	0.24	0.029	0.569	0.013
50	0.25	0.68	0.27	0.35	0.063	0.695	0.019
55	0.35	0.79	0.32	0.46	0.064	0.827	0.018
60	0.37	0.83	0.31	0.5	0.069	0.922	0.020
65	0.38	0.87	0.24	0.54	0.070	1.02	0.023
70	0.43	0.94	0.25	0.63	0.072	1.11	0.024
75	0.46	0.98	0.29	0.67	0.075	1.14	0.025
80	0.48	0.97	0.26	0.73	0.092	1.21	0.026
85	0.52	1.04	0.28	0.81	0.108	1.21	0.022

E_e (eV)	CF_2^+	$CH_2F_2^+$	CHF_2^+	CF^+	CHF^+	CH_2F^+	Total
20	0.08	0.26	0.18	0.02	0.12	2.35	4.89
25	0.17	0.61	0.42	0.09	0.42	6.59	13.00
30	0.25	0.83	0.56	0.17	0.75	10.01	19.37
35	0.32	0.96	0.65	0.24	0.99	12.80	24.51
40	0.37	1.11	0.73	0.3	1.22	15.16	29.04
45	0.39	1.15	0.77	0.35	1.41	16.95	32.36
50	0.41	1.2	0.81	0.38	1.56	18.29	34.90
55	0.46	1.25	0.82	0.42	1.73	19.20	36.98
60	0.47	1.24	0.84	0.45	1.81	20.02	38.45
65	0.5	1.26	0.85	0.47	1.86	20.66	39.52
70	0.51	1.28	0.85	0.49	1.92	21.15	40.56
75	0.53	1.25	0.85	0.5	1.96	21.39	41.10
80	0.55	1.27	0.86	0.52	2.06	21.81	41.91
85	0.57	1.27	0.86	0.54	2.15	22.26	42.88

sensitive to high kinetic energy ions. Indeed, some ions are lost before the extraction pulse is applied and those accelerated later spread considerably while travelling to the detector and eventually reaching a geometric cross section larger than that of the detector area, so that some ions escape detection. Hence, part of the signal is lost and the measured ionization cross sections are smaller than expected. Nevertheless, as light fragment cross sections are very small, the signal loss does not significantly affect the total ionization cross section. Pressure, measured with an accuracy of 1%, is also a minor error source. Overall errors are estimated to be less than 10% for ions with a mass similar to that of the reference, increasing to 20% for the lighter fragments.

3.2. Appearance potential measurements

AP thresholds of the most significant ions produced by electron impact on CH_2F_2 were measured by recording the ionization signal as a function of the electron impact energy and extrapolating to zero signal; examples for CF_2^+, CF^+, C^+ and CH^+ ions are shown in figure 6. The Ar^+ ionization signal profile (AP $=$ 15.75 eV) is also included in the plots to scale the electron energy and to eliminate contact potentials, which are significant in fluorinated

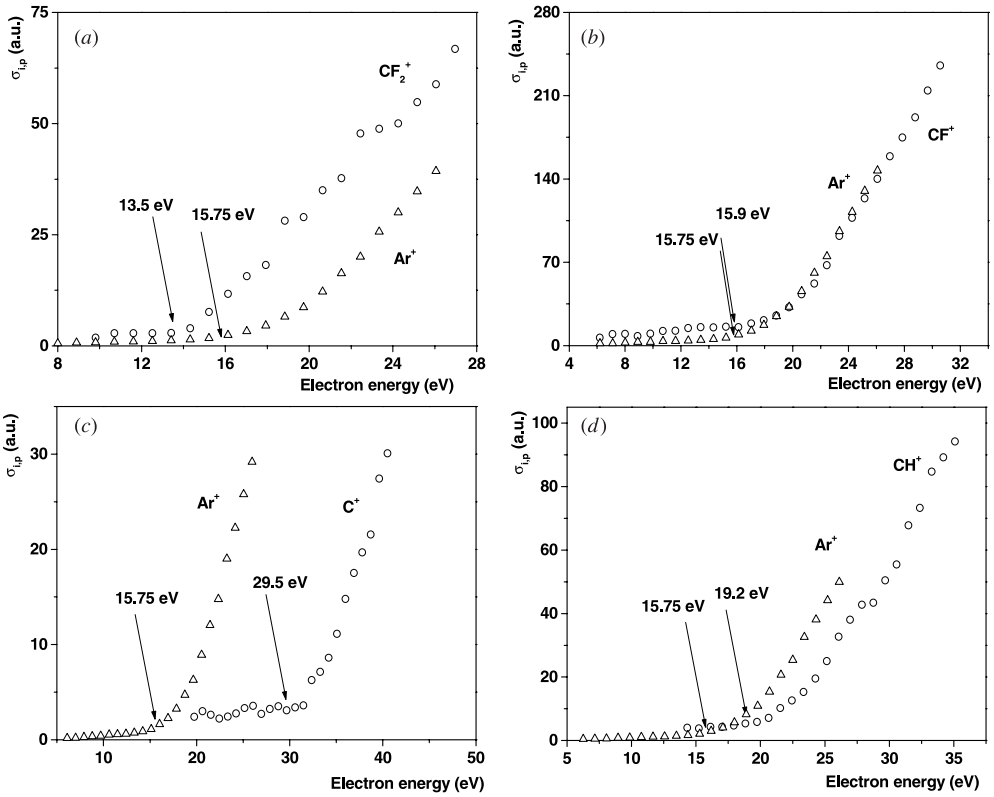

Figure 6. Appearance potentials of a few positive ions arising in the electron impact on CH_2F_2. The selected ions are: (*a*) CF_2^+, (*b*) CF^+, (*c*) C^+ and (*d*) CH^+. The Ar^+ threshold is used as a standard to calibrate the electron energy (IP $Ar^+ = 15.75$ eV). The list of the appearance potentials measured in this work is presented in table 2.

compounds (Müller *et al* 1992). The CH_2F_2 ionization signal traces are characterized by long tails, extending for as much as several eV, and although many suggestions have been forwarded to justify them, they seem to originate from the electron-emitting cathode voltage drop. Moreover, both the presence of the extraction field in the collision volume and the parent vibrational excited states favour the dissociation process and contribute to decreasing the energy onset; consequently, some channel assignments are equivocal, though there are cases where the threshold law aids in solving the ambiguity (Märk 1995). Ionization measurements were performed at the lowest electron intensity compatible with a sizeable signal, in order to diminish the ion energy spread to the maximum. In our system the energy spread at 10 μA electron current is about 0.6–0.8 eV decreasing to 0.5 eV for 1 μA. CF_4 and CHF_3 APs have been compared with those obtained by electron energy selector methods (Märk and Torres 2000) and in both cases the agreement is excellent.

The electron impact ionization channels on target CH_2F_2 are depicted in table 2 and are mismatched to the experimental APs. Fragment heats of formation from JANAF tables (Lide 1985), and other standard data collections (Lide 1992–3, Tarnovsky and Becker 1993) have been used to calculate the AP presented in the third column of the table. In order to reduce the number of channels, only vibrational and electronic ground states have been assumed to be produced. Errors in the calculations are estimated to be $\pm$0.8–1.0 eV.

Table 2. Correlation between the ionization channels, referred to by a channel number, the calculated and the experimental thresholds for the most significant ion fragments produced by electron impact on CH_2F_2. Experimental threshold errors are estimated to be ± 1 eV.

Channel no	Ionization pathway	Calculated threshold (eV)	Appearance potential (eV)	Other measurements
1	$CH_2F_2 \rightarrow CH_2F_2^+$		12.6	12.71[a] 12.6[b]
2	$CH_2F_2 \rightarrow CHF_2^+ + H$	**13.10**	12.8	13.11[c] 13.14[d] 13.1[b]
3	$CH_2F_2 \rightarrow CH_2F^+ + F$	**14.43**	14.9	14.06[c] 15.28[b]
4	$CH_2F_2 \rightarrow CHF^+ + HF$	**13.63**	13.3	
5	$\rightarrow CHF^+ + H + F$	19.54		17.7[b]
6	$CH_2F_2 \rightarrow CF_2^+ + H_2$	**13.98**	13.5	14.8[e]
7	$\rightarrow CF_2^+ + H + H$	18.50		
8	$CH_2F_2 \rightarrow CF^+ + HF + H$	**15.86**	15.9	
9	$\rightarrow CF^+ + F + H_2$	17.25		18.8[b]
10	$\rightarrow CF^+ + F + 2H$	21.76		
11	$CH_2F_2 \rightarrow CH^+ + HF + F$	**19.46**	19.2	
12	$\rightarrow CH^+ + H + F_2$	23.72		
13	$\rightarrow CH^+ + F + 2F$	25.37		
14	$CH_2F_2 \rightarrow CH_2^+ + F_2$	19.07		
15	$\rightarrow CH_2^+ + 2F$	**20.71**	23.9	
16	$CH_2F_2 \rightarrow C^+ + 2HF$	17.71		
17	$\rightarrow C^+ + H_2 + F_2$	23.36		
18	$\rightarrow C^+ + HF + H + F$	23.62		
19	$\rightarrow C^+ + H_2 + 2F$	25.00		
20	$\rightarrow C^+ + 2H + F_2$	27.87		
21	$\rightarrow C^+ + 2H + 2F$	**29.52**	29.5	
22	$CH_2F_2 \rightarrow F^+ + CH_2F$	22.60		
23	$\rightarrow F^+ + CF + H_2$	25.56		
24	$\rightarrow F^+ + CH + HF$	26.25		
25	$\rightarrow F^+ + CHF + H$	26.48		
26	$\rightarrow F^+ + CH_2 + F$	27.74		
27	$\rightarrow F^+ + C + HF + H$	29.78		
28	$\rightarrow F^+ + CF + 2H$	30.08		
29	$\rightarrow F^+ + C + H_2 + F$	31.17		
30	$\rightarrow F^+ + C + F + 2H$	**35.68**	34.3	

[a] Lias (1988).
[b] Lifshitz and Long (1965).
[c] Lossing (1972).
[d] Martin *et al* (1966).
[e] Steele (1964).

In table 2, the first channel yields an experimental threshold of 12.6 ± 1.0 eV for the $CH_2F_2^+$ ion, within the experimental uncertainties, in excellent agreement with those reported by Lias (1988) (12.71 eV), and Lifshitz and Long (1965) (by electron impact, 12.6 eV). Channels 2 and 3 produce CHF_2^+ and CH_2F^+ ions, respectively; in the former the C–H bond dissociation energy amounts to 3.49 eV (Herzberg and Johns 1969) whilst 5.5 eV is needed to dissociate the C–F bond and yields CH_2F^+ (Gaydon 1968). The energy bonds difference matches that of the AP (2.3 eV) and demonstrates that both ions proceed through a common pathway, where the energy excess produces either the C–H bond (12.8 eV for CHF_2^+ formation) or the C–F bond dissociation (14.9 eV for CH_2F^+ formation), with negligible kinetic energy difference.

The channels leading to CHF^+, CF_2^+ and CF^+ ions show specific properties; to begin with, in the most likely channels, the ions' partners are molecular fragments, i.e. HF for the CHF^+ and CF^+ ions, and H_2 for CF_2^+, in contrast with the dissociation channels leading to excited species, where the likely fragment partners are ground state atoms (Martínez *et al* 1992, Donohue *et al* 1977). A similar behaviour is observed for the CH^+ ion, with an onset at 19.2 ± 1.0 eV and HF and F as partners. Nevertheless, it should be pointed out that the lightest fragments and, in general, no fluorine ions, come out from the ionization process with higher kinetic energy, implying higher AP than those calculated (table 2). The effect is straightforward in the CH_2^+ formation, where the AP is 23.9 ± 1.0 eV and the nearest channel differs by more than 3 eV. Consequently, a KED detailed study is required to establish an adequate description of the dissociative ionization process.

3.3. Nascent kinetic energy distributions

Nascent KEDs were computed from the TOF-MS band profiles (Franklin *et al* 1967, Schäfer *et al* 1991, equation (1)) and the relevant results for the set of detected ions at selected electron impact energies are plotted in figure 7. The agreement between the CF_4 fragment KEDs obtained and those reported by Christophorou *et al* (1996) leads us to estimate error limits of less than 20% (Torres *et al* 2000). In most cases the electron impact energy increase does not imply significant changes in the KED, implying very close or at least energetically similar processes. The heaviest ions studied including CF^+, CF_2^+, CHF^+, CH_2F^+, CHF_2^+ and $CH_2F_2^+$ show, as a general feature, very low kinetic energies—of the order of a few tenths or even hundredths of an eV average energy. Heavy fragment velocities perpendicular to the supersonic molecule/electron beam plane are expected to be small, as confirmed experimentally.

The H^+, C^+, CH^+, CH_2^+ and F^+ light and medium mass ion group displays a large variety of KED behaviour, with energy maxima in the 1–5 eV range and in some cases higher (8–10 eV). Fragments appearing with high kinetic energies result from the detachment of heavy fluorine atoms from the parent molecule, where they constitute more than 70% of the total molecular mass. Removal of light ions is prone to be associated with a considerable kinetic energy.

The knowledge of KEDs and the previously discussed AP allows a better and more accurate channel identification. To begin with, the heavier ion APs ($CH_2F_2^+$, CHF_2^+, CH_2F^+, CHF^+, CF_2^+ and CF^+) shown in table 2 are close to the calculated ones. Consequently, heavier ion fragments will arise with no or small kinetic energy, as KEDs depicted in figure 7 effectively show. Inspection of the mass spectrum intensities leads to identify the CH_2F^+ ion as the most abundantly produced in the dissociative ionization process. Nevertheless, $CH_2F_2^+$ and CHF_2^+ ions appear at lower incident electron energy and their KEDs show a maximum close to 0 eV followed by a tail extending to some hundredths of eV, whereas the CH_2F^+ ion has a maximum of around 0.3 eV. The observation suggests that the CH_2F^+ is produced from a $CH_2F_2^+$ repulsive state, located at about 14 eV, and the small energy excess is taken by the nascent ion. In contrast, $CH_2F_2^+$ and CHF_2^+ ions seem to originate from a similar channel for a parent molecule bonding electronic state close to 12.6 eV (see the orbital energy discussion below).

Among the KED studied those for CH_2^+ and CH^+ at low electron impact energies are of particular relevance and singularity: both ions have band profiles with split satellite peaks and, consequently, negative and positive slopes (cf figure 4). The central peak is associated with a narrow quasithermal ion energy distribution, whilst the side bands originate from detachments with relatively high nascent translational energy (Franklin *et al* 1967). Figure 7 shows both KEDs and peak maxima at electron impact energies of 47 and 83 eV, respectively.

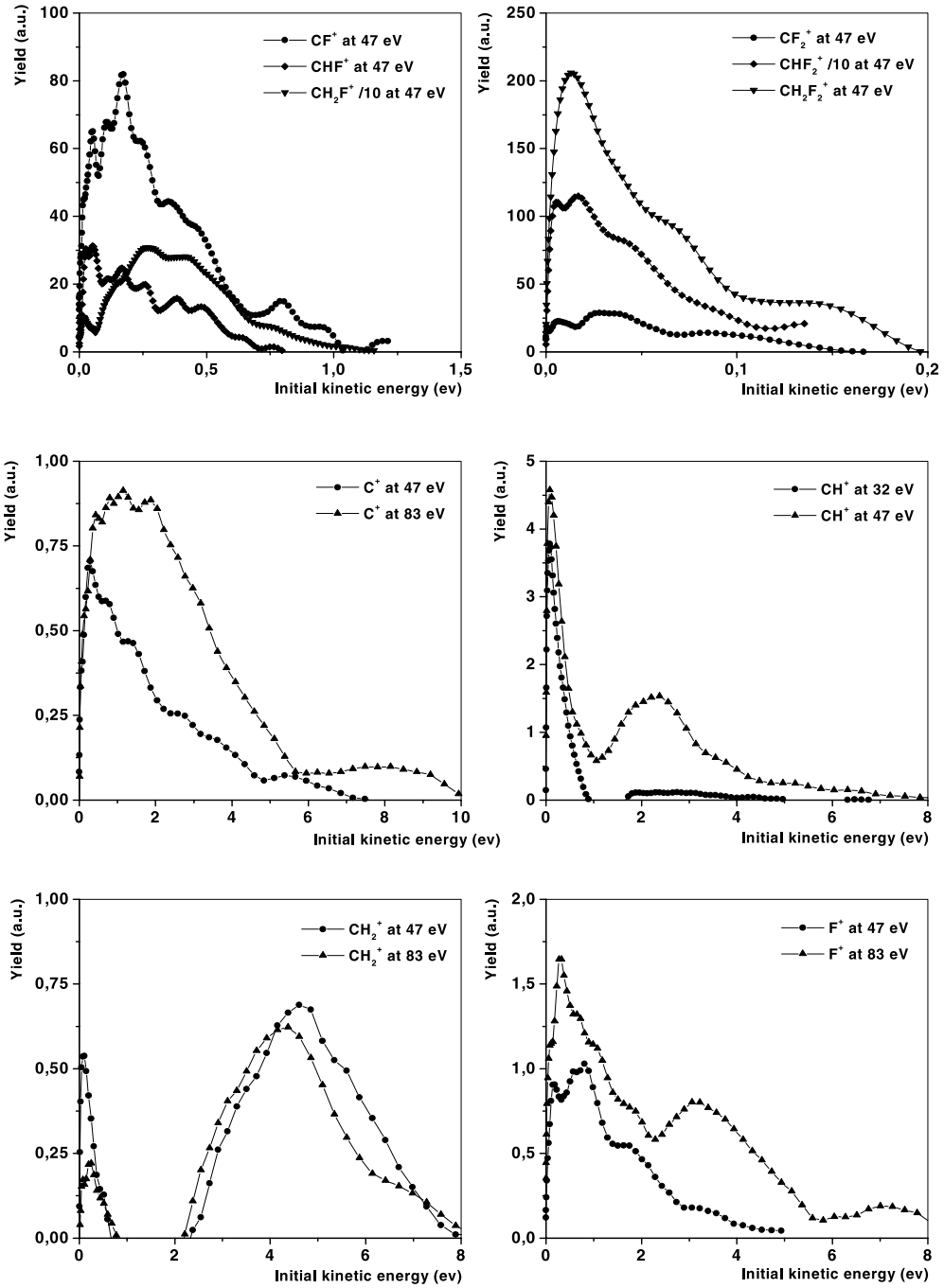

Figure 7. Kinetic energy distributions of CF^+ (at 47 eV), CHF^+ (at 47 eV), CH_2F^+ (at 47 eV, factor of $\frac{1}{10}$), CF_2^+ (at 47 eV), CHF_2^+ (at 47 eV, factor of $\frac{1}{10}$), $CH_2F_2^+$ (at 47 eV), C^+ (at 47 and 83 eV), CH^+ (at 32 and 47 eV), CH_2^+ (at 47 and 83 eV) and F^+ (at 47 and 83 eV) ions produced by electron impact dissociative ionization on the CH_2F_2 parent molecule. Note that the ion KEDs in the two upper plots are in the 0–1.5 and 0–0.2 eV range.

At low electron impact energy, the F^+ ion KED has negligible contributions above 1.5 eV, and the energy balance indicates that the leading dissociation channel is that labelled as 30 in table 2, yielding an F^+ ion and a full atomization. At electron impact energies over threshold a new peak centred at 3 eV appears in the KE distribution (figure 7). The plausible opening of a new channel associated with the new peak is not mirrored in the absolute partial or the total cross section profiles (cf figure 5), likely to be due to either the opening of a new channel with a cross section similar to that of channel 30 or to the production of F^+ ions with high kinetic energy in the same channel. Under the former hypothesis, the closest channel in energy is number 29 (31.17 eV), with the 4.5 eV energy excess shared between the channel products' kinetic energies. Although channel 29 is closest in energy, it may well be that other pathways contribute to F^+ ion production, but to a lesser proportion.

In the production of the C^+ ion, the higher the electron impact energy the higher the kinetic energy (the maximum changes from 0.3 to 2 eV). At low incident electron energy, channel 21 is expected to control the C^+ formation. By comparison with the F^+ ion production process, the C^+ would proceed via full atomization of the CH_2F_2 precursor. An electron impact energy increase presumably opens other dissociation channels, as may be the case of channel 20 differing by 1.7 eV from channel 21, and producing faster C^+ ions.

The CH_2^+ ion shows a KED maximum around 5 eV even at low electron impact energy, suggesting that the $CH_2F_2^+$ electronic states leading to CH_2^+ are dominated by repulsive states. Bearing in mind the broad nascent ion kinetic energy distributions it seems likely that channels 14 and 15 (table 2) contribute to the CH_2^+ formation. It should also be remembered that since only velocities directed to and from the detector contribute to band broadening, ions observed with zero kinetic energy correspond not only to quasithermal fragments but also to ions with kinetic energy in the molecular–electron beam plane. With respect to the CH^+ ion, the sharp peak observed in the KED following low electron impact energy leads to identifying channel 11 (19.5 eV) as the starting channel of thermal fragments. At higher incident electron energy, a KED maximum appears at ~ 2.5 eV due to either the production of faster CH^+ ions by the same pathways or to the opening of additional dissociation channels. The sharp peak observed around 0 eV kinetic energy dominates the distribution over all the incident electron energy range and no observable onsets appear in the ionization cross section plot, leading one to assume that the production of faster CH^+ ions by the same pathways is the more reliable one. However, a more detailed study on molecular orbital energies will provide additional insight into the dissociation process and will suggest the opening of a new channel above 36 eV, yielding fast CH^+ ions.

Two additional observations on dissociation channels deserve attention: the ions' partner fragments and the neutral fragments' total kinetic energy. In the case of heavier ions created with low kinetic energy, their favoured partners are molecules (channels 4, 6 and 8), while the production of ionized atoms requires the full dissociation of the parent molecule (channels 21 and 30). The CH^+ ion and, above all, CH_2^+ constitute intermediate cases where the correct assignment becomes challenging since kinetic energy plays an important role and often more than one channel might contribute to yield the same ion. In all cases the dissociation pathway corresponding to the threshold energy dominates the ionization process regardless of the electron impact energy as no shoulders are observed in the ionization cross sections. For any specific ion dissociation channel, the ion/neutrals must fulfil the linear momentum and kinetic energy conservation principles in the plane perpendicular to the electron–molecule beams. The ions and neutrals total kinetic energy (W_{exc}) is related to that of the ion kinetic energy (W_{ion}) of mass M^+ by the equation (Poll and Meichsner 1987):

$$W_{\mathrm{ion}} = (1 - M^+/M_N)W_{\mathrm{exc}}$$

where M_N denotes the parent molecule mass. In dissociation pathways yielding light ions ($M^+/M_N \ll 1$) the kinetic energy release is mainly taken by the light ion and the corrections carried out above do not significantly affect the arguments put forward in the present discussion.

3.4. Molecular orbitals and dissociation pathways

CH_2F_2 experimental ionization thresholds are now analysed along with the adiabatic and vertical potentials determined by 'high-resolution' He I and He II photoelectron spectroscopy (Brundle *et al* 1970, Pullen *et al* 1970) and with the computed *ab initio* molecular orbital energies carried out by Gaussian 98W at the RHF/6-311+G* level (Gaussian 98W, 1998) Computed ionization potentials were obtained from Koopman's theorem, and the resulting overestimated values corrected by an 0.85 factor (Brundle *et al* 1970). For convenience these experimental and computed values are collected in table 3. Identifying ion formation pathways is not a trivial task and requires information from other experimental techniques. The ion appearance potential (table 2) is an upper limit of the computed thermodynamic value, since fragments might arise not only from direct dissociative ionization but from different excited states of the parent molecule, as autoionization states (Märk 1984), Coulomb implosions in the case of precursor multiple ionization, ionization of clusters, etc. These effects are usually small for low electron impact energy, so that comparing the theoretical and the experimental results shown in tables 2 and 3 may still infer worthwhile conclusions about the electron orbital involved in the process.

Table 3. Orbital nomenclature, *ab initio* (Gaussian 98W RHF/6-311G*) calculated orbital energies, corrected Koopmans' ionization potential, experimental adiabatic ionization potential and experimental vertical ionization potential (Brundle *et al* 1970) (in eV) for the CH_2F_2 molecule.

Molecular orbital	Orbital energy (eV)	Calculated IP × 0.85	Adiabatic IP (eV)	Vertical IP (eV)
$2b_2$	−14.64	12.44	12.72	13.27
$6a_1$	−17.06	14.5		
$4b_1$	−17.32	14.72	⩾14.5	15.3
$1a_2$	−18.29	15.55		15.71
$3b_1$	−20.87	17.74		
$5a_1$	−21.33	18.13	18.20	18.9
$1b_2$	−21.53	18.3		
$4a_1$	−26.61	22.62	23.1	23.9
$2b_1$	−43.85	37.27		
$3a_1$	−45.66	38.81		

The opening of channel 1 happens at an electron impact energy of 12.6 eV, a value close to that of the C–H bonding and C–F antibonding $2b_2$ orbital adiabatic ionization potential (Brundle *et al* 1970). The ejection of the electron will lead to a stable $(2b_2)^{-1}$ $CH_2F_2^+$ state, and is observed in the mass spectra (figure 3) with a relatively small but sizeable cross section all over the energy range (table 1).

Dissociation channels 2, 4 and 6 must also come from withdrawing one electron from the $2b_2$ orbital, since the energy required to switch on these channels lies below those of either $6a_1$ or $4b_1$ orbitals: $CH_2F_2^+$ appearance will proceed through Franck–Condon transitions at high vibrational levels, where part of the energy is rearranged among the numerous degrees of freedom. According to the quasiequilibrium theory (QET) (Märk 1984), molecular ion decomposition occurs after a period long enough for the energy stored in one degree of

freedom to equal the dissociation energy. Energy rearrangements within the $CH_2F_2^+$ ion were first suggested by Brundle *et al* (1970), who discussed the CHF_2^+ formation as a result of an autoionization process or an internal energy transfer to the fragment vibrational modes below that of the ground state of the parent ion, populated by a Franck–Condon allowed transition.

The CH_2F^+ ionization threshold matches, within experimental error, the necessary energy to remove one electron from either $6a_1$ or $4b_1$ molecular orbitals, as both are close in energy. The orbital $6a_1$ is C–H bonding and C–F antibonding, so that withdrawing one electron will lead to $CH_2F_2^+$ in a more stable state than the extraction of one electron from the pure C–F bonding $4b_1$ orbital. The excitation to unstable or strongly dissociative states leads to a lower $CH_2F_2^+$ ionization cross section than for most fragments. Furthermore, the CH_2F^+ fragment has a wider KED than that of CHF_2^+ or CF_2^+, suggesting a different formation pathway. The comparison of $6a_1$ and $4b_1$ orbital properties leads to identifying the $4b_1$ orbital as more dissociative and hence it is proposed as the key to open channel 3.

The energy to open channel 8 is close to 15.9 eV, in agreement with that required to remove one electron from the $1a_2$ orbital (≈ 15.6 eV). This orbital has neither a bonding nor an antibonding character for any of the bonds involved in the process of dissociation. Thus, the electron in this orbital is non-bonding and the nascent ion, CF^+, will arise with low kinetic energy.

At 19.2 ± 1 eV the CH^+ ion begins to be observed and this onset is close to the electron extraction energy from the $5a_1$ orbital (18.2 eV). The $5a_1$ orbital has both C–F and C–H bonding character (0.114 and 0.069, respectively) and, in spite of the lack of experimental values, the theoretical predictions suggest that both $3b_1$ and $1b_2$ orbital energies are close to that of the $5a_1$ orbital, giving rise to strongly repulsive $CH_2F_2^+$ states. $3b_1$, $5a_1$ and $1b_2$ orbitals have an increasing bonding character and, as a result, the CH^+ ion arising from these channels will come out with increasingly higher kinetic energies. At incident electron energy over 36 eV a change in the KED is observed, appearing a maximum at 2 eV (figure 6). Table 3 also shows that the $2b_1$ orbital has an energy close to that of the fast ion threshold, so that the removal of one electron might lead to more energetic CH^+ distributions through a different channel. At higher incident electron energies more and more channels are open and contribute to the formation of the ion.

Channel 15 is associated with the formation of the CH_2^+ ion and correlates with the removal of one electron from the $4a_1$ orbital (23.1 eV according to Brundle *et al* (1970)). The KED of CH_2^+ has a maximum at 4–5 eV, that added to the thermodynamic calculated energy of 20.71 eV, yields a value in agreement with the experimental onset for channel 15 (23.9 ± 1 eV) and also with the mainly bonding character of the $4a_1$ orbital. However, channel 14, with a slight smaller onset of 19.07 eV, might also be a good channel candidate for the creation of the ion.

Finally, it should be pointed out that the other channels referred to in table 2 do not seem to correlate with any CH_2F_2 molecular orbital. The nearest deeper orbital to $4a_1$ is $2b_1$, with an ionization energy of 37.3 eV, a value higher than the energy involved in any of the 20, 21, 29 and 30 channels. There are no vertical ionization potential data for energies over 28 eV (Brundle *et al* 1970). In addition, channels 20, 21, 29 and 30 yield C^+ and F^+ ions and a large number of atoms, involving a considerable amount of energy required for the parent total dissociation. The mechanisms are more complex and might arise from CH_2F_2 multiple-ionized state Coulomb implosions that would explain the fragments high kinetic energies. Besides, some C^+ or F^+ partners might be ions, and the energy required for the dissociation would be lower than that stated in table 2. Multiple ionization would also confirm the presence of neutral fragments as partners of the considered ion.

Acknowledgments

We are grateful to the DGES, MEC (Madrid) for partial support of this work through grants PB95-0510 and PB96-1472. Also to the Gobierno Vasco (Vitoria) for co-financial support grants and to the UPV for a three-year (1998–2000) Research Group Grant. One of us (IT) thanks the Gobierno Vasco (Vitoria) for the award of a post-graduate Fellowship and for funds for a visit to Professor T D Märk's laboratory (Innsbruck, Austria).

References

Bonham R A 1994 *Japan. J. Appl. Phys.* **33** 4157
Bruce M R and Bonham R A 1993 *Int. J. Mass Spectrom. Ion Process.* **123** 97
Brundle C R, Robin M B and Basch H 1970 *J. Chem. Phys.* **53** 2196
Christophorou L G and Olthoff J K 1998a *J. Phys. Chem. Ref. Data* **27** 1
——1998b *J. Phys. Chem. Ref. Data* **27** 889 and references therein
Christophorou L G, Olthoff J K and Rao M V V S 1996 *J. Phys. Chem. Ref. Data* **25** 1341
——1997a *J. Phys. Chem. Ref. Data* **26** 1 and references therein
Christophorou L G, Olthoff J K and Wang Y 1997b *J. Phys. Chem. Ref. Data* **26** 1205 and references therein
Donohue D E, Schiavone J A and Freund R S 1977 *J. Chem. Phys.* **67** 769
Frankin J I, Hierl P M and Wran D A 1967 *J. Chem. Phys.* **47** 3148
Frisch M J *et al* 1998 *Gaussian 98* Revision A.3 (Pittsburgh, PA: Gaussian)
Gaydon A G 1968 *Dissociation Energies and Spectra of Diatomic Molecules* 3rd edn (London: Chapman and Hall)
Herzberg G J and Johns J W G 1969 *Astrophys. J.* **158** 399
Lias S G 1988 Gas-phase ion and neutral thermochemistry *J. Phys. Chem. Ref. Data* **17** no 1
Lide D R (ed) 1992–3 *Handbook of Chemistry and Physics* 73rd edn (Boca Raton, FL: Chemical Rubber Company)
——1985 *JANAF Thermochemical Tables* 3rd edn *J. Phys. Chem. Ref. Data* **14** no 1
Lifshitz C and Long F A 1965 *J. Chem. Phys.* **69** 3731
Märk T D 1984 *Electron–Molecule Interactions and their Applications* ed L G Christophorou vol 1 (Orlando, FL: Academic) ch 3
——1995 *Atomic and Molecular Processes in Fusion Edge Plasmas* ed R K Janev (New York: Plenum) pp 69 and 298
Märk T D and Torres I 2000 in preparation
Martínez R, Castaño F and Sánchez Rayo M N 1992 *J. Phys. B: At. Mol. Opt. Phys.* **25** 4951
Martínez R, Castaño F, Sánchez Rayo M N and Pereira R 1993 *Chem. Phys.* **172** 349
Moss S J and Ledwith A ed 1987 *The Chemistry of the Semiconductor Industry* (Glasgow: Blackie)
Müller U, Bubel T, Schulz G, Sevilla A, Dike J and Becker K 1992 *Z. Phys.* D **24** 131
Poll H U and Meichsner J 1987 *Contrib. Plasma Phys.* **27** 359
Poll H U, Winkler C, Margreiter D, Grill V and Märk T D 1992 *Int. J. Mass Spectrom. Ion Process.* **112** 1
Pullen B P, Carlson T A, Moddeman W E, Schweitzer G K, Bull W E and Grimm F A 1970 *J. Chem. Phys.* **53** 768
Roth J R 1995 *Industrial Plasma Engineering* vol 1 (Bristol: IOP Publishing)
Schäfer K, Baek W Y, Föster K, Gassen D and Neuwirth W 1991 *Z. Phys.* D **21** 137
SIMION-3D, version 3.0 1987 Idaho National Engineering Laboratory (Idaho Falls, ID: EG&G Idaho Inc.)
Stephan K, Helm H and Märk T D 1980 *J. Chem. Phys.* **73** 3763
Straub H C, Renault P, Lindsay B G, Smith K A and Stebbings R F 1995 *Phys. Rev.* A **52** 1115
——1996 *Phys. Rev.* A **54** 2146
Straub H C, Lindsay B G, Smith K A and Stebbings R F 1998 *J. Chem. Phys.* **108** 109
Syage J A 1988 *Chem. Phys. Lett.* **143** 19
Tarnovsky V and Becker K 1993 *J. Chem. Phys.* **98** 7868
Tarnovsky V, Deutsch H, Martus K E and Becker K 1998 *J. Chem. Phys.* **109** 6596 and references therein
Tarnovsky V, Levin A, Becker K, Basner R and Schdmidt M 1994 *Int. J. Mass Spectrom. Ion Proc.* **133** 175
Torres I, Martínez R, Sánchez Rayo M N, Fernández J A and Castaño F 1999 *J. Phys. B: At. Mol. Opt. Phys.* **32** 5437
Torres I, Martínez R, Sánchez Rayo M N and Castaño F 2000 *Chem. Phys. Lett.* at press
Wayne R P 1991 *Chemistry of Atmospheres* 2nd edn (Oxford: Clarendon)
Wetzel R C, Baiocchi F A, Hayes T R and Freund R S 1987 *Phys. Rev.* A **35** 559
Wiley W C and McLaren I H 1955 *Rev. Sci. Instrum.* **26** 1150